UNIVERSITI
MALAYSIA
PERLIS

UniMAP

Doping of Erbium(III) Oxide Nanoparticles–Polymer Interfaces in Biodegradable Inorganic Solid Polymer Electrolytes for Enhanced Ionic Conductivity

Mee Yoke Chong[1*], YCY Evyan[2], N. Zebardastan[3], K. Kumar[4], K. Ramesh[5] and S. Ramesh[5]

[1]Centre for American Education, INTI International University, Persiaran Bandar Baru Nilai, 71800 Nilai, Malaysia.
[2]Faculty of Applied Sciences, Nilai University, Persiaran Bandar Baru Nilai, 71800 Nilai, Malaysia.
[3]Queensland University of Technology, 2 George St, Brisbane City QLD 4000, Australia.
[4]INTI College Nilai, Persiaran Bandar Baru Nilai, 71800 Nilai, Malaysia.
[5]Centre for Ionics University of Malaya, Department of Physics, University of Malaya, 50603 Kuala Lumpur, Malaysia.

ABSTRACT

The severity of the environmental issue, caused by the heavy consumption of fossil fuel encourages the development of biodegradable energy storage devices. Electrolyte, which provides charge carriers, is one of the basic component in constructing an energy storage device. Hence, a solution casting technique has been adopted to prepare biodegradable inorganic solid polymer electrolyte (SPE) which contains hydroxylethyl cellulose (biodegradable host polymer), magnesium trifluoromethane sulfonate (charge carriers) and 1-ethyl-3-methylimidazolium trifluoromethane sulfonate ionic liquid (plasticizer). Unfortunately, it portrays low ionic conductivity which will lead to the drop in the performance of the energy storage device. Therefore, a study is conducted to observe the ionic conductivity of the SPE upon doping of various percentage of erbium(III) oxide (Er_2O_3) nanoparticles. It is found that the SPE doped with 2 wt. % erbium(III) oxide nanoparticles obtained the highest ionic conductivity at room temperature (4.02×10^{-4} S/cm). The result is well in agreement with the high dielectric permittivity owing to the great Lewis interaction between the charge carrier and nanoparticles.

Keywords: Biodegradable, Inorganic, Ionic Conductivity, Rare-earth Nanoparticles, Solid Polymer Electrolyte.

1. INTRODUCTION

Climate change is creating a greater consciousness among the international community. It emerges exponentially with the consumption of fossil fuel which creates irreparable impact to the environment. The severity of the environmental issue motivates the use of biodegradable materials in response to conserve mother nature [1]. Hence, Chai & Isa (2016) employed carboxymethyl cellulose as host polymer for solid polymer electrolyte (SPE). Additionally, Jurgensen *et al.,* (2016) mentioned that the preparation of SPE for energy and electrochromic devices arise from degradable sources such as cellulose and its derivatives, starch, chitosan, carrageenan and agarose [2]. To date, the usage of biodegradable polymer as the host in the SPE for energy storage device never ceases. Researchers innovate the SPE by preparing biodegradable-based blend polymers in order to improve the ionic conductivity as well as to have excellent mechanical stability. Shujahadeen *et al.,* (2019) prepared blend polymers of chitosan/methyl cellulose and chitosan/dextran for the carbon based supercapacitor that possess high ionic conductivity of 2.81×10^{-3} S/cm and 1×10^{-3} S/cm, respectively [3–4]. On the

[*]Corresponding Author: meeyoke.chong@newinti.edu.my

other hand, poly (vinyl alcohol) was blended with proline for the primary proton battery and fuel cell along with high ionic conductivity of 7.01 x 10^{-4} S/cm [5].

Regrettably, the blend polymer of PVA/poly (N-vinyl pyrrolidone) (PVP) for solid-state lithium battery obtained slightly low ionic conductivity (1.15 x 10^{-5} S/cm) [6]. Therefore, the utilization of hydroxylethyl cellulose (HEC) as host polymer in this study is inspired by the properties of green polymers which suppress the detrimental effect on the environment. Moreover, the presence of abundant hydroxyl groups which lead to the increase of two lone pair electrons per hydroxyl group provides a robust platform for adsorption of charge carriers [7–9].

The SPE portrays outstanding safety features (i.e. leakage, and thermal stability) and less cumbersome handling process compared to liquid and gel polymer electrolyte [10]. However, it is impeded by the low ionic conductivities at room temperature which is an essential parameter for an ideal SPE [11]. Nanoparticles play a noteworthy role in improving the conductivities coupled with good mechanical stability compared to their counterpart remedies (i.e. polymer blending or copolymerization and incorporation of ionic liquid and plasticizers) [12]. Researchers resort to various nanoparticles such as Al_2O_3, CuO, $BaTiO_3$ and etc. for better interfacial compatibility between charge carriers and host polymer [13–14]. At present, Zhang *et al.,* (2019) and Vasudevan & Fullerton-Shirey (2019) accentuate the unique features of nanoparticles by synthesizing 5 nm $BaTiO_3$ nanoparticles and ellipse TiO_2 nanoparticles, respectively, for the SPE of the energy storage device. In fact, the shaped nanoparticles boost the conductivity with a small amount of powder as well as enhance better dispersion with the host polymer [15–16]. Likewise, Kumar *et al.,* (2017) explored the use of copper-constantan (copper-nickel alloy) nanoparticles for the lithium battery. The ionic conductivity of the SPE improved to 1.0 x 10^{-4} S/cm [17]. The idea of incorporating silver nanoparticles which is meant to prevent the aggregation of ions and retain the amorphous phase of the polymer matrix is attempted by Morsi *et al.,* (2018). This is apart from its promising properties (i.e. optical, magnetic and electrical) in the field of material science [18].

Thereafter, the incorporation of Er_2O_3, a rare earth nanoparticle into the SPE is interesting because it is not employed widely in the preparation of SPE for the energy storage device. The unique properties of Er_2O_3 nanoparticles is amplified through ~~the~~ its use in the field of energy storage devices (i.e. solar cells, supercapacitor and sensors) and optical communications and optoelectronics [19–20]. Arya and co-workers (2018) compared the conductivity of the SPEs upon addition of cerium(IV) oxide and Er_2O_3 nanoparticles. It was found that the inclusion of 10 wt. % of Er_2O_3 nanoparticles into the non-biodegradable blend polymer (PEO/PVC) attained the highest ionic conductivity (2.3 x 10^{-5} S/cm) [21]. Subsequently, the doping of Er_2O_3 nanoparticles is chosen in this study because it is capable to enhance the surface area of the polymer matrix for greater adsorption of charge carriers apart from it being low in toxicity and has a greater range of chemical and physical behaviour [22–23].

In this study, various wt. % of Er_2O_3 nanoparticles is doped with HEC, magnesium trifluoromethane sulfonate ($MgTf_2$) and 1-ethyl-3-methylimidazolium trifluoromethane sulfonate (EMIMTf) by using the solution casting technique. The impedance spectroscopy is used to investigate the conductivities and dielectric properties of the SPEs at various wt. % of Er_2O_3 nanoparticles. On top of that, X-Ray diffractometer is used to explore the amorphocity of the polymer matrix upon inclusion of Er_2O_3 nanoparticles.

2. MATERIAL AND METHODS

2.1 Preparation of Inorganic SPE Film

The chemicals, namely, hydroxylethyl cellulose polymer, magnesium trifluoromethane sulfonate salt, 1-ethyl-3-methylimidazolium trifluoromethane sulfonate ionic liquid and erbium(III) oxide nanoparticles were purchased from Sigma–Aldrich, USA. The polymer and salt were dried in the oven whereas the nanoparticles were activated in accordance to the method reported by Taghizadeh & Seifi-Aghjekohal (2015) for better dispersion prior to use [24]. The polymer, salt, ionic liquid and nanoparticles were dissolved in deionized water and it was stirred continuously for 24 hours at room temperature. Following this, the homogeneous solution was cast on a Teflon coated aluminium foil and allowed to evaporate at 70℃. A thin and opaque film of inorganic SPE was formed. The compositions and designations for the prepared inorganic SPE film is summarized in Table 1. Also, Figure 1 summarizes the flow of the methodology in this research.

Table 1 Compositions and designations of SPE complexes

Compositions (wt. %) $HEC: MgTf_2: EMIMTf: E_2O_3$	Designations of SPEs
48.0: 12.0: 40.0: 0.0	H0
47.2: 11.8: 40.0: 1.0	HE1
46.4: 11.6: 40.0: 2.0	HE2
45.6: 11.4: 40.0: 3.0	HE3
44.8: 11.2: 40.0: 4.0	HE4

2.2 Characterizations

The thickness of the film was measured using the Mitutoyo micrometer screw gauge. Ionic conductivity and dielectric measurement were performed by using HIOKI 3532-50 LCR HiTESTER, over a frequency range between 50 Hz and 5 MHz. Samples were sandwiched between stainless steel (SS) blocking electrodes under spring pressure with the configuration of SS/SPE/SS as shown in Figure 2. Also, the conductivity-temperature study was conducted in the temperature range of 30–120 °C.

The equations for the ionic conductivities (σ_s), dielectric permittivity (ε') and dielectric loss (ε'') can be shown as follows [25]:

$$\sigma_s = \frac{L}{R_b A} \tag{1}$$

Where L is the thickness in cm, R_b is the bulk resistance in Ω, and A is the area of the blocking electrode in cm².

$$\varepsilon' = \frac{Z_i}{\omega C_o (Z_r^2 + Z_i^2)} \tag{2}$$
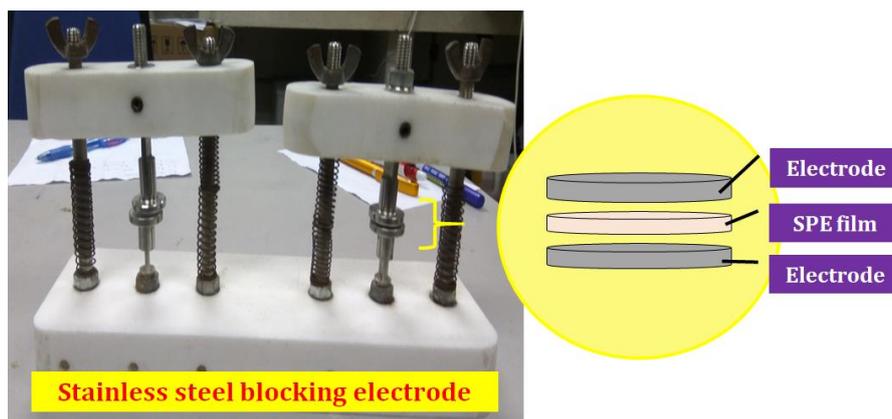
Where Z_i is imaginary impedance in Ω, Z_r is real impedance, C_o is the absolute permittivity (8.85 x 10⁻¹² F/m) and ω is the angular frequency in s⁻¹.

$$\varepsilon'' = \frac{Z_r}{\omega C_o (Z_r^2 + Z_i^2)} \tag{3}$$

XRD patterns of SPEs were measured using Siemens D5000 diffractometer with Cu–Kα radiation (λ = 1.5406 Å).
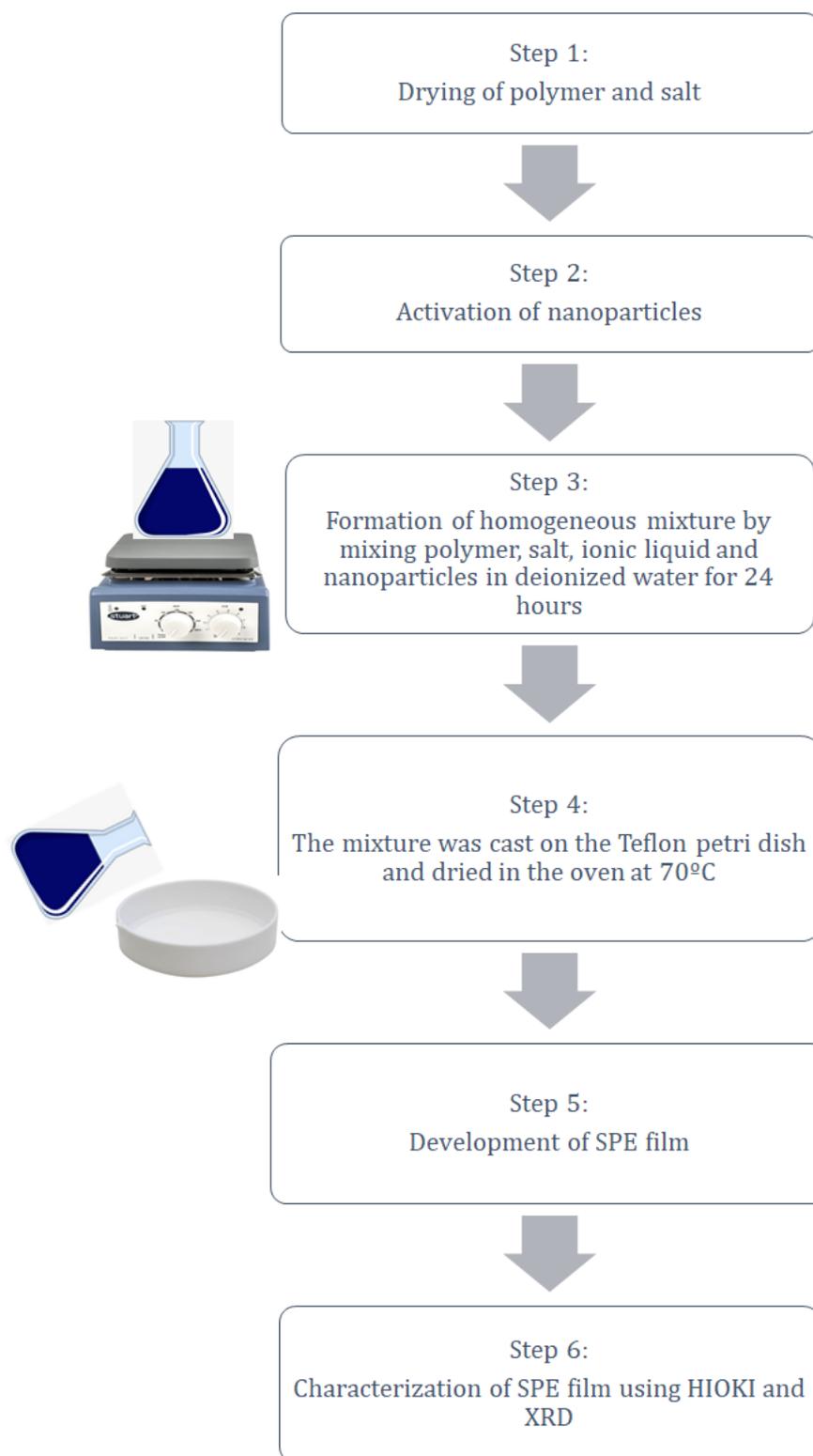
Figure 1. The flow of the research methodology.

**Figure 2.** The stainless steel blocking electrode used to sandwich the SPE film for conductivity analysis.

3. RESULTS AND DISCUSSION

3.1 Conductivity Analysis

Figure 3 shows the variation of ionic conductivities at room temperature for SPEs (without and with the addition of nanoparticles). Based on Figure 3, the filler-free SPE obtained an ambient ionic conductivity of 9.28 x 10^{-5} S/cm due to the primary interaction between charge carriers and host polymer. The ambient ionic conductivities of the SPEs increased continuously to 1.14 x 10^{-4} S/cm and 4.02 x 10^{-4} S/cm upon the addition of 1 and 2 wt. % of nanoparticles, respectively. HE1 owned restricted sites for adsorption of charge carriers [26]. Hence, it experienced low ambient ionic conductivities of 1.14 x 10^{-4} S/cm. HE2 achieved the most optimum ionic conductivity at room temperature because the nanoparticles exhibited the magnificent Lewis acid – base interaction with the charge carriers. At high wt. % of nanoparticles, the ambient ionic conductivities of the SPEs were depressed because the transportation of mobile charge carriers was hindered by the aggregation of nanoparticles. Subsequently, the ambient ionic conductivities of both HE3 and HE4 decreased to 2.98 x 10^{-4} S/cm and 1.79 x 10^{-4} S/cm, respectively [27].
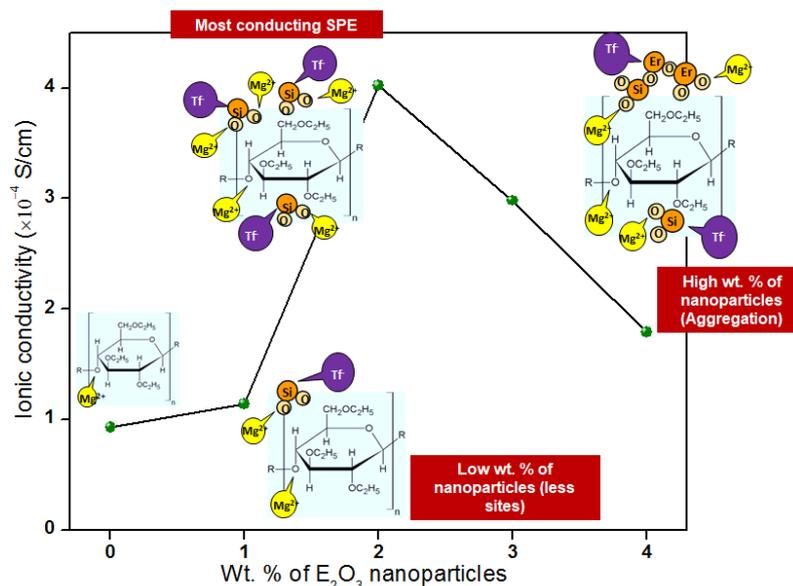
Figure 3. The variation of ionic conductivities at room temperature for SPEs (without and with the addition of nanoparticles).
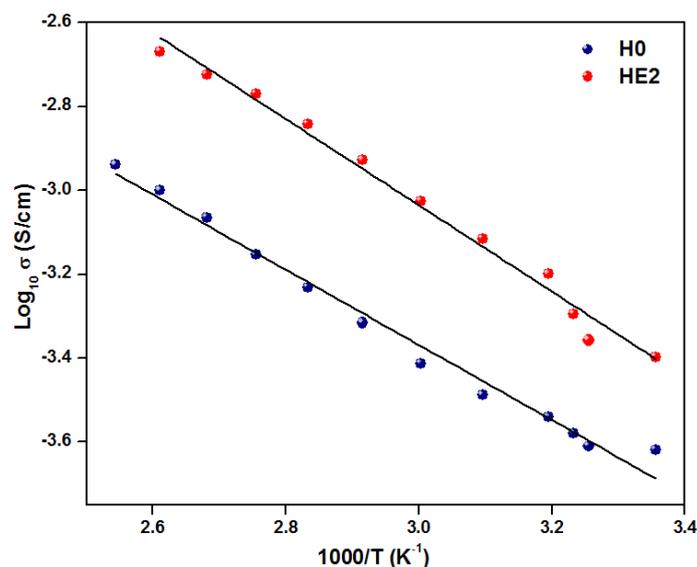
Figure 4. The temperature dependence of ionic conductivities for H0 and HE2 (most conducting SPE).

Figure 4 describes the temperature dependence of ionic conductivities for H0 and HE2 (the most conducting SPE). The linear line disclosed the absence of phase transition from semi–crystalline to amorphous along with the regression values (R^2) close to unity. Both H0 and HE2 obtained R^2 values of 0.9897 and 0.9856, respectively. Undoubtedly, all the SPEs obeyed Arrhenius theory as articulated by Balo *et al.,* (2017) [28]. As the temperature increased, the expansion of polymer chain integrated well with the rise in effective collision among the charge carriers which led to the raise in their kinetic energy [29].

3.2 Dielectric Spectra

Figures 5(a) and (b) depict the variation of dielectric permittivity and dielectric loss with logarithm frequency, respectively for H0 and HE2 (most conducting SPE). Generally, the dielectric permittivity dwindled, and an irregular pattern of dielectric loss was observed with the increased frequency for all the SPEs. The electrode polarization effect elevated upon the incorporation of 2 wt. % of erbium(III) oxide nanoparticles in low frequency region (50 Hz – 1 kHz). The electrodes were charged when current was applied to them and thus more dipoles were polarized at appropriate orientation [30]. As a consequence, HE2 obtained the highest ε' and ε'' values of 1.3×10^5 and 3.3×10^4, respectively. At moderate frequency regions (1 kHz – 100 kHz), HE2 led the molecular polarization effect because the ε' value is higher than H0. There were more molecules in HE2 polarized through weak intermolecular forces such as Van der Waals forces, permanent dipoles and ion-dipole forces caused by effective collision occurred among the charge carriers. Referring to Figure 5(b), broad relaxation peaks were observed upon incorporation of 2 wt. % nanoparticles. As a consequence, heat energy is dissipated under the influence of alternating current electric field [31–32]. At a high frequency region (100 kHz – 5 MHz), both the dielectric permittivity and dielectric loss of the SPEs dropped to a plateau region because the ions were unable to orientate with the current applied [33].
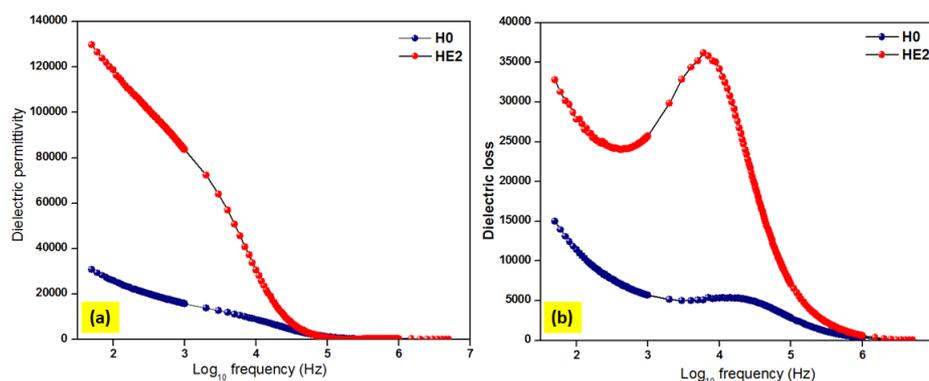
Figure 5. The variation of (a) dielectric permittivity and (b) dielectric loss with logarithm frequency for H0 and HE2 (most conducting SPE).

3.3 XRD Analysis

Figure 6 shows the XRD patterns of pure samples (HEC and erbium(III) oxide nanoparticles), H0 and HE2 (most conducting SPE). A pure HEC has two humps at $2\theta = 9°$ and $22°$. However, the hump at $2\theta = 8°$ was absent in both H0 and HE2 owing to the presence of plasticizers, that occurred upon the incorporation of ionic liquid [34]. On the other hand, a pure erbium(III) oxide nanoparticles have three sharp peaks at $2\theta = 29°$, $34°$ and $49°$ which contributed to the (2 2 2), (4 0 0), (5 1 0) crystal planes of crystalline erbium(III) oxide nanoparticles (JCPDS card no. 01-077-0459) [35]. These peaks were seen in HE2 which indicates successful incorporation of erbium(III) oxide to the SPE via solution casting technique. Although the XRD diffractogram shows that HE2 is a bit crystalline upon doping of erbium(III) oxide nanoparticles compared to H0, the nanoparticles do not obstruct the transportation of charge carriers. This is because of the small size of the nanoparticles.

Figure 7 depicts the interaction and role of nanoparticles in the SPE. The host polymer, HEC, acts as the backbone for the adsorption of Mg^{2+} ions via ion-dipole force due to the presence of abundant hydroxyl groups. The transportation is further enhanced by the Lewis acid-base interactions with the ions. The small size of nanoparticles filled up the space in the polymer matrix and hence, the partially positive charge (Er^{3+}) serves as the Lewis acid to attract the Tf^- ions. Similarly, partially negative charge (O^{2-}) of the nanoparticles serves as the Lewis base to attract the Mg^{2+} ions. In short, HE2 achieves high ionic conductivity due to the transportation of both Mg^{2+} and Tf^- ions.
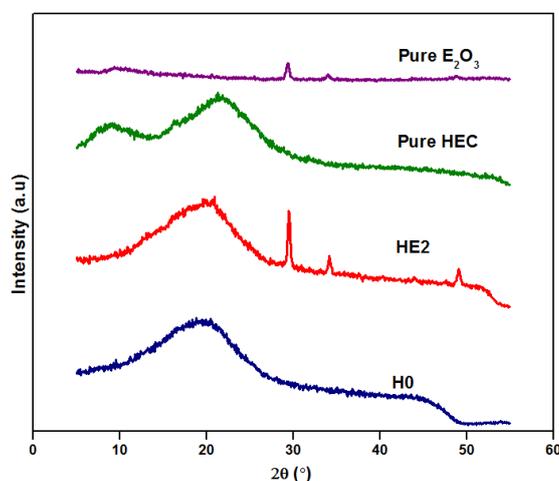
Figure 6. XRD patterns of pure samples (HEC and erbium(III) oxide nanoparticles), H0 and HE2 (most conducting SPE).
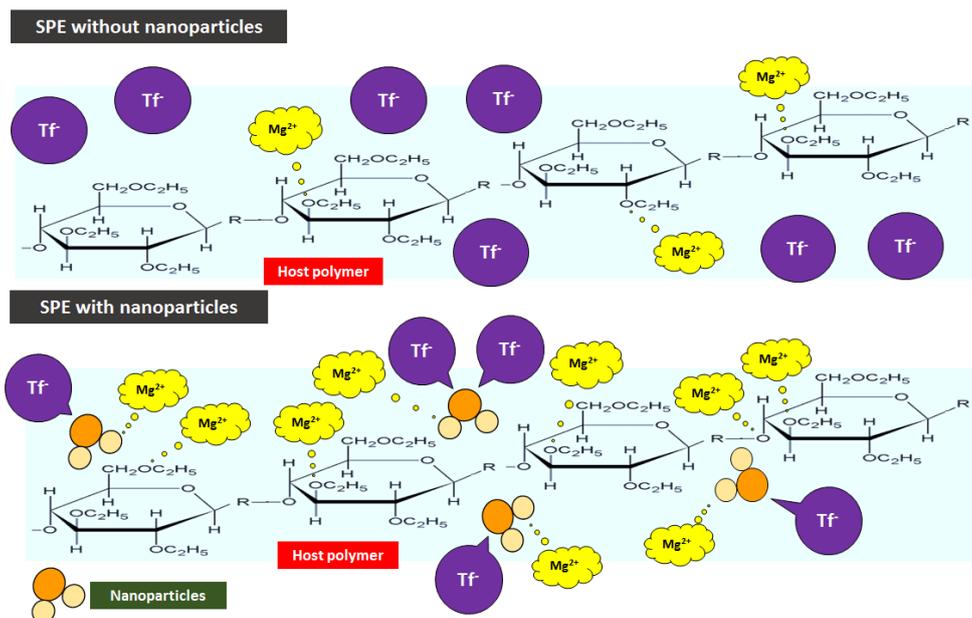
Figure 7. The interactions of the charge carriers in the SPEs (without and with nanoparticles).

4. CONCLUSION

The biodegradable SPE was prepared using the solution casting technique. The SPE doped with 2 wt. % of erbium(III) oxide portrayed the highest ionic conductivity and dielectric permittivity value of 4.02 x 10^{-4} S/cm and 1.3×10^5. respectively. Although, the HE2 SPE is slightly crystalline owing to the peaks observed at 2θ = 29°, 34° and 49°, it doesn't hinder the transportation of charge carriers along the polymer matrix. This is because the small size of the nanoparticles filled the space in the polymer matrix. Subsequently, the role of the nanoparticles become more prominent owing to the increase in the ionic conductivity. The conductivity was enhanced by the transportation of Tf^- and Mg^{2+} ions through the Lewis acid-base between nanoparticles and salt apart from polymer and salt.

ACKNOWLEDGEMENTS

REFERENCES

[1]   M. Chai, M. Isa, Scientific Reports **6** (2016) 27328.
[2]   N. Jürgensen, J. Zimmermann, A. J. Morfa, G. Hernandez-Sosa, Scientific Reports **6** (2016) 36643.
[3]   S. B. Aziz, M. Hamsan, R. M. Abdullah, M. Kadir, Molecules **24** (2019) 2503.
[4]   S. B. Aziz, M. Hamsan, W. O. Karim, M. Kadir, M. Brza, O. G. Abdullah, Biomolecules **9** (2019) 267.
[5]   R. Hemalatha, M. Alagar, S. Selvasekarapandian, B. Sundaresan, V. Moniha, G. Boopathi, P. C. Selvin, Ionics **25** (2019) 141.

[6]   K. Deshmukh, M. B. Ahamed, A. R. Polu, K. K. Sadasivuni, S. K. Pasha, D. Ponnamma, M. A. AlMaadeed, R. R. Deshmukh, K. Chidambaram, Journal of Materials Science: Materials in Electronics **27** (2016) 11410.
[7]   P. Khare, R. Pandey, P. Jain, Bulletin of Materials Science **23** (2000) 325.
[8]   B. J. Kong, A. Kim, S. N. Park, Carbohydrate Polymers **147** (2016) 473.
[9]   J. Zheng, S. Jung, P. W. Schmidt, T. P. Lodge, T. M. Reineke, ACS Macro Letters **6** (2017) 145.
[10]   Y. Zhao, C. Wu, G. Peng, X. Chen, X. Yao, Y. Bai, F. Wu, S. Chen, X. Xu, Journal of Power Sources **301** (2016) 47.
[11]   O. Garcia-Calvo, N. Lago, S. Devaraj, M. Armand, Electrochimica Acta **220** (2016) 587.
[12]   S. Ganesan, K. Mothilal, T. Ganesan, Ionics **24** (2018) 3845.
[13]   C. Ma, J. Zhang, M. Xu, Q. Xia, J. Liu, S. Zhao, L. Chen, A. Pan, D. G. Ivey, W. Wei, Journal of Power Sources **317** (2016) 103.
[14]   S. Choudhary, R. Sengwa, Electrochimica Acta **247** (2017) 924.
[15]   S. Vasudevan, S. K. Fullerton-Shirey, The Journal of Physical Chemistry C **123** (2019) 10720.
[16]   Y. Zhang, X. Wang, W. Feng, Y. Zhen, P. Zhao, L. Li, Z. Cai, Journal of Solid State Electrochemistry **23** (2019) 749.
[17]   K. N. Kumar, K. Saijyothi, L. Vijayalakshmi, M. Kang, Polymer Bulletin **74** (2017) 2545.
[18]   M. Morsi, S. A. El-Khodary, A. Rajeh, Physica B: Condensed Matter **539** (2018) 88.
[19]   M. Azlan, M. Halimah, A. Suriani, Y. Azlina, S. Umar, R. El-Mallawany, Optics Communications **448** (2019) 82.
[20]   W. Que, Y. Zhou, Y. Lam, K. Pita, Y. Chan, C. Kam, Applied Physics A **73** (2001) 209.
[21]   A. Arya, M. Sadiq, A. Sharma, Ionics **24** (2018) 2295.
[22]   P. L. Kharel, F. P. Zamborini, B. W. Alphenaar, Journal of The Electrochemical Society **165** (2018) H52.
[23]   R. Umamaheswari, S. Manavalan, S. M. Chen, S. Chinnapaiyan, T. W. Chen, R. J. Ramalingam, Ultrasonics Sonochemistry **56** (2019) 422.
[24]   M. T. Taghizadeh, P. Seifi-Aghjekohal, Ultrasonics Sonochemistry **26** (2015) 265.
[25]   M. Y. Chong, C. W. Liew, A. Numan, K. Yugal, K. Ramesh, H. M. Ng, T. V. Chong, S. Ramesh, Ionics **22** (2016) 2421.
[26]   R. Galindo, E. Mazario, S. Gutiérrez, M. Morales, P. Herrasti, Journal of Alloys and Compounds **536** (2012) S241.
[27]   J. M. C. Puguan, W. J. Chung, H. Kim, Electrochimica Acta **196** (2016) 236.
[28]   L. Balo, H. Gupta, V. K. Singh, R. K. Singh, Electrochimica Acta **230** (2017) 123.
[29]   N. Farhana, M. H. Khanmirzaei, S. Ramesh, K. Ramesh, Journal of Applied Polymer Science **134** (2017) 45091.
[30]   M. Hema, P. Tamilselvi, Journal of Physics and Chemistry of Solids **96** (2016) 42.
[31]   P. Yadav, A. K. Srivastava, M. K. Yadav, R. Kripal, V. Singh, D. B. Lee, J. H. Lee, Arabian Journal of Chemistry **12** (2015) 440.
[32]   M. S. Zheng, J. W. Zha, Y. Yang, C. Q. Li, P. Han, C. H. Hu, Y. Q. Wen, Z. M. Dang, Polymer **130** (2017) 258.
[33]   K. Anbazhakan, S. Selvasekarapandiyan, S. Monisha, M. Premalatha, A. Neelaveni, Ionics **23** (2017) 2663.
[34]   M. Y. Chong, A. Numan, C. W. Liew, H. M. Ng, K. Ramesh, S. Ramesh, Journal of Physics and Chemistry of Solids **117** (2018) 194.
[35]   F. Azad, A. Maqsood, Electronic Materials Letters **10** (2014) 557.